frontiers | Frontiers in Marine Science

ORIGINAL RESEARCH
published: 13 July 2022
doi: 10.3389/fmars.2022.944841

Impact of High Methane Flux on the Properties of Pore Fluid and Methane-Derived Authigenic Carbonate in the ARAON Mounds, Chukchi Sea

Ji-Hoon Kim[1], Myong-Ho Park[2], Dong-Hun Lee[3], Hirotsugu Minami[4], Young-Keun Jin[5], Akihiro Hachikubo[4], Jin Hur[6], Jong-Sik Ryu[7], Moo-Hee Kang[1], Kwangchul Jang[8], Masato Kida[4], Yongwon Seo[9], Meilian Chen[10], Jong Kuk Hong[5], Yungoo Song[11] and Sanghee Park[12]*

[1] Marine Geology and Energy Division, Korea Institute of Geoscience and Mineral Resources, Daejeon, South Korea, [2] CCS Research Center, Kongju National University, Gongju, South Korea, [3] Marine Environment Research Division, National Institute of Fisheries Science, Busan, South Korea, [4] Environmental and Energy Resources Research Center, Kitami Institute of Technology, Kitami, Japan, [5] Division of Earth Sciences, Korea Polar Research Institute, Incheon, South Korea, [6] Department of Environment and Energy, Sejong University, Seoul, South Korea, [7] Department of Earth and Environmental Sciences, Pukyong National University, Busan, South Korea, [8] Division of Glacier Environment Research, Korea Polar Research Institute, Incheon, South Korea, [9] Department of Urban and Environmental Engineering, Ulsan National Institute of Science and Technology, Ulsan, South Korea, [10] Environmental Program, Guangdong Technion - Israel Institute of Technology, Shantou, China, [11] Department of Earth System Sciences, Yonsei University, Seoul, South Korea, [12] Division of Earth and Environment Sciences, Korea Basic Science Institute, Cheonju, South Korea

OPEN ACCESS

Edited by:
Jörn Peckmann, University of Hamburg, Germany

Reviewed by:
Niu Li, South China Sea Institute of Oceanology (CAS), China
Claudio Argentino, UiT The Arctic University of Norway, Norway

***Correspondence:**
Ji-Hoon Kim
save@kigam.re.kr

Specialty section:
This article was submitted to Marine Biogeochemistry, a section of the journal Frontiers in Marine Science

Received: *15 May 2022*
Accepted: *07 June 2022*
Published: *13 July 2022*

Citation:
Kim J-H, Park M-H, Lee D-H, Minami H, Jin Y-K, Hachikubo A, Hur J, Ryu J-S, Kang M-H, Jang K, Kida M, Seo Y, Chen M, Hong JK, Song Y and Park S (2022) Impact of High Methane Flux on the Properties of Pore Fluid and Methane-Derived Authigenic Carbonate in the ARAON Mounds, Chukchi Sea. Front. Mar. Sci. 9:944841. doi: 10.3389/fmars.2022.944841

We investigated the pore fluid and methane-derived authigenic carbonate (MDAC) chemistry from the ARAON Mounds in the Chukchi Sea to reveal how methane (CH_4) seepage impacts their compositional and isotopic properties. During the ARA07C and ARA09C Expeditions, many *in situ* gas hydrates (GHs) and MDACs were found near the seafloor. The fluid chemistry has been considerably modified in association with the high CH_4 flux and its related byproducts (GHs and MDACs). Compared to Site ARA09C-St 08 (reference site), which displays a linear SO_4^{2-} downcore profile, the other sites (e.g., ARA07C-St 13, ARA07C-St 14, ARA09C-St 04, ARA09C-St 07, and ARA09C-St 12) that are found byproducts exhibit concave-up and/or kink type SO_4^{2-} profiles. The physical properties and fluid pathways in sediment columns have been altered by these byproducts, which prevents the steady state condition of the dissolved species through them. Consequently, chemical zones are separated between bearing and non-bearing byproducts intervals under non-steady state condition from the seafloor to the sulfate-methane transition (SMT). GH dissociation also significantly impacts pore fluid properties (e.g., low Cl^-, enriched δD and $\delta^{18}O$). The upward CH_4 with depleted $\delta^{13}C$ from the thermogenic origin affects the chemical signatures of MDACs. The enriched $\delta^{18}O$ fluid from GH dissociation also influences the properties of MDACs. Thus, in the ARAON Mounds, the chemistry of the fluid and MDAC has significantly changed, most likely responding to the CH_4 flux and GH dissociation through geological time. Overall,

our findings will improve the understanding and prediction of the pore fluid and MDAC chemistry in the Arctic Ocean related to CH_4 seepage by global climate change.

Keywords: pore fluid, methane flux, gas hydrate, MDAC, ARAON Mounds

INTRODUCTION

Methane (CH_4) seepages (cold seeps) migrating from deep sediment to the seafloor have widely occurred along continental margins (Campbell, 2006; Judd and Hovland, 2007; Suess, 2014 and references therein). However, most of the CH_4 released by this mechanism is consumed in the sediments and/or in the water column before reaching the atmosphere (Boetius et al., 2000; Boetius and Wenzhöfer, 2013). Nevertheless, it has been reported that an annual approximately 0.4-12.2 Tg CH_4 is discharged into the water column by the methane seepage (Judd et al., 2002), which can provide enough CH_4 to form gas hydrates (GHs) and carbonates on the seafloor and to change seafloor morphology. As a result, methane seepages contribute to the global carbon cycles as well as marine geology and (bio)geochemistry.

Recently, the cryosphere extent (e.g., ice sheet, permafrost, and glaciers) in Arctic regions has been continuously reduced due to rapid temperature increases compared to those in other regions. Therefore, numerous methane releases related to submarine permafrost and GH degradation have been reported in the Arctic regions, e.g., the Eastern Siberian Arctic Shelf, offshore Svalbard, and the Chukchi Sea (Shakhova et al., 2005; Westbrook et al., 2009; Shakhova et al., 2010; Hong et al., 2017). The shrinkage of the cryosphere extent is expected to accelerate continuously in the future, releasing a large amount of CH_4. This CH_4 released from the sediment column will play a critical positive feedback role in global warming, marine geology, (bio)geochemistry, and microbial activities, linked to the ebullition of gas transport (Schuur et al., 2015; Argentino et al., 2021; Kim et al., 2021a; Lee et al., 2021; Sauer et al., 2021).

Elevated bathymetric features from a few meters to kilometers in diameter, simply called mounds, have been observed on the seafloor (e.g., Chapman et al., 2004; Bahr et al., 2007; Buerk et al., 2010; Römer et al., 2014; Koch et al., 2015). These structures are prominent conduits for the transport of deep hydrocarbons to the seafloor, where many seafloor gas vents and GHs are observed (Paull et al., 2008; Römer et al., 2014; Hong et al., 2017; Waage et al., 2019). During the ARA07C Expedition, many GHs were found on the seafloor of the ARAON Mounds (water depth of ~600 m) located in the Chukchi Sea (Kim et al., 2020; Choi et al., 2021). Kim et al. (2020) revealed that the CH_4 in GHs primarily originates from deep thermogenic gas, which is upwardly transported to the seafloor through fractures and/or faults in this mound and influences the compositional and isotopic properties of the gases differently between GH-bearing and non-GH bearing sediments. The CH_4 that migrates to the seafloor can be oxidized by microbes, either aerobically near the sediment-water interface, or anaerobically in the subsurface (Barnes and Goldberg, 1976; Reeburgh, 1976), which can alter the (geo/bio) chemical properties of pore fluid and microbial activities. In particular, the anaerobic oxidation of methane (AOM) in the sulfate-methane transition (SMT) increases dissolved sulfide and alkalinity in pore fluid, which in turn provides energy for chemosynthetic symbionts (Paull et al., 1984; Sibuet and Olu, 1998; Sahling et al., 2002) and precipitates methane-derived authigenic carbonates (MDACs), respectively (Aloisi et al., 2000; Luff et al., 2004; Bayon et al., 2009; Himmler et al., 2011; Himmler et al., 2015). Indeed, many *in situ* MDACs have been observed in the ARAON Mounds during the ARA07C Expedition (Jin and Shipboard Scientific Party, 2017; Kim et al., 2020). Consequently, gas seepage and its associated byproducts (i.e., GH and MDAC) can remarkably alter the pore fluid chemistry in the ARAON Mounds. However, to date, the fluid chemistry associated with these mounds has not been investigated. As a result, it is not clear how gas seepage and its associated byproducts impact regional hydrology, alter the chemical properties of pore fluids, and interact with pore fluids under current and past global climate changes.

Here, we investigate two questions to decipher the pore fluid chemistry in the ARAON Mounds: 1) how methane seepage from deep-seated sediment impacts the fluid properties and 2) how GHs and MDACs interact with pore fluid. In addition, no data exist on the chemical and biomarker signatures of MDACs found at the ARAON Mounds. To unravel these questions, we first investigate the compositional and isotopic properties of pore fluid and MDAC from three sampling site groups in the ARAON Mounds: 1) a reference site (ARA09C-St 08) without methane seepage, 2) GH bearing sites (ARA07C-St 13, ARA09C-St 06, ARA09C-St 16), and 3) non-GH bearing sites (ARA07C-St 14, ARA09C-St 04, ARA09C-St 07, and ARA09C-St 12) with methane seepage (**Figure 1**). Our findings will improve the understanding and prediction of fluid and MDAC chemistry linked with methane seepage from deep-seated sediments to the seafloor in the Arctic Ocean.

REGIONAL SETTINGS

The Chukchi Sea extends from 66°N in the south to the edge of the Arctic Basin in the north, covering an area of 620,000 km^2 (Jakobsson, 2002). In this sea, the Chukchi Shelf encompasses a shallow continental margin north of Chukotka and Alaska is less than 50 m depth in the south, to 450-750 m depth at the shelf break around the northward extension known as the Chukchi Rise. The Chukchi Borderland is an adjacent fragment of continental crust extending north into the Canada Basin of the Arctic Ocean (Grantz et al., 1998), which incorporates the Northwind Ridge and the Chukchi Plateau (**Figure 1**).

The study area, the ARAON Mounds, has a relatively gentle slope (approximately 2°) with a > 3 km wide terrace, as shown in the multibeam data, and eight mound structures have been observed along the edge of the terrace between water depths of 568 m to 704 m by the sub-bottom profiler (SBP) image (**Figure 1**) Jin and Shipboard Scientific Party, 2017; Jin and Shipboard Scientific Party, 2019). These mounds are named ARAON Mound 01 to 08 (AM01 to AM08) from northwest to southeast, and they are approximately 10 m higher than the surrounding seafloor with 200-700 m in diameter (**Figure 1**). In addition, the SBP image shows that the acoustic facies,

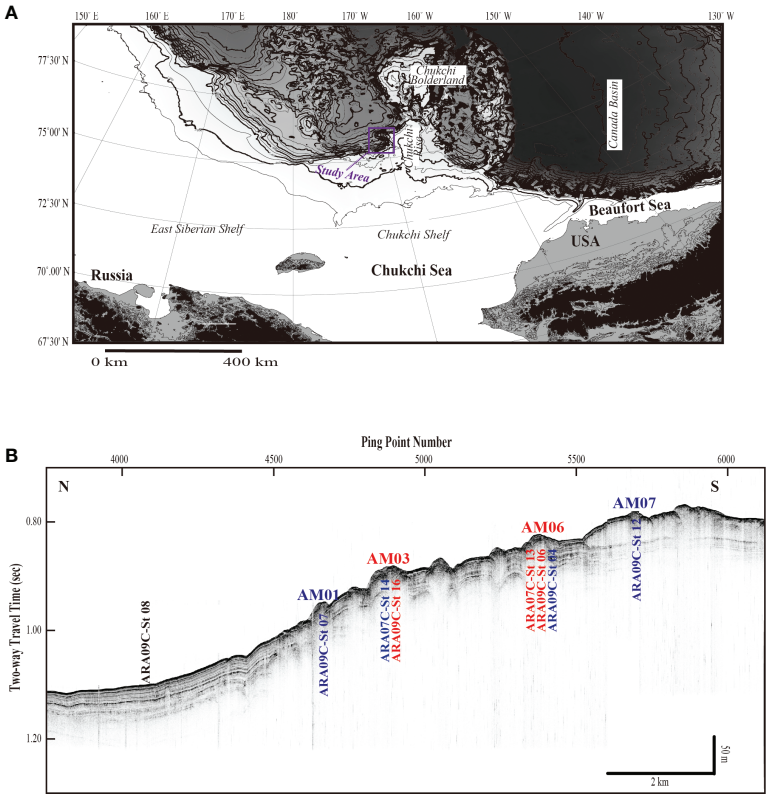

FIGURE 1 | (A) Major physiographic features and locations of the study area during the ARA07C and ARA09C Expeditions. **(B)** Sub-bottom profile (SBP) images of the ARAON Mounds (AMs) surveyed during the ARA09C Expedition. Black color site: reference site without GHs and MDACs, blue color sites: observation of MDACs, and red color sites: observation of GHs and MDACs.

stratigraphy, and structure of the subsurface are different at each mound (**Figure 1**) because of the different behavior of thick transparent facies interbedded in the stratified facies (Jin and Shipboard Scientific Party, 2017; Jin and Shipboard Scientific Party, 2019; Kim et al., 2021b). In terms of acoustic characteristics and tectonic views, the ARAON Mounds seem to form in association with basin bounding-faults by prolonged seepage and to be active at this stage (Kim et al., 2021b).

MATERIALS AND METHODS

Fluid and MDAC Sampling

Two gravity cores (GCs; ARA07C-St 13 and ARA07C-St 14) and five GCs (ARA09C-St 04, ARA09C-St 06, ARA09C-St 07, ARA09C-St 12, and ARA09C-St 16) were collected from the ARAON Mounds during the ARA07C Expedition in 2016 and the ARA09C Expedition in 2018 onboard Ice-Breaking Research Vessel (*IBRV*) ARAON, respectively. In addition, one GC was sampled at Site ARA09C-St 08 as a reference site. The retrieved core length of all GCs is less than 6 m (**Figure 1**; **Table 1**).

Pore fluid was extracted by Rhizons in whole round cores or split cores in ~10-60 cm intervals at room temperature on the *IBRV* ARAON. Extracted pore fluid was collected in acid-prewashed syringes equipped with an in-line 0.20 μm disposable polytetrafluoroethylene filter. The bottom seawater was also collected from Site ARA09C-St 04 (**Table 1**) using a CTD/rosette system that holds 12-5L Niskin bottles (Seabird 911 Plus). Fluid subsamples for shipboard and anion analyses were collected in acid-prewashed high-density polyethylene (HDPE) bottles. Fluid aliquots for cation and $^{87}Sr/^{86}Sr$ isotope ratios analyses were transferred into acid-prewashed HDPE bottles (~2-4 ml) and acidified with 20 μl ultrapure grade HNO_3. Subsamples for stable isotopic properties of water (δD and $\delta^{18}O$) and dissolved inorganic carbon ($\delta^{13}C_{DIC}$) were collected in 2 ml septum screw-lid glass vials. Fluid samples for $\delta^{13}C_{DIC}$ analysis were preserved with 30 μl $HgCl_2$. Pore fluid and seawater samples were stored at approximately 4°C in the refrigerator until the analyses.

Gas hydrates from Sites ARA07C-St 13, ARA09C-St 06, and ARA09C-St 16 were carefully scraped to minimize any contamination that may have occurred during the earlier handling and were dissociated in clean 20 ml glass beakers at room temperature on the *IBRV* ARAON. The aliquots of these fluids (hydrate-bound waters) for the analyses of compositional and isotopic properties were collected using the same techniques as described above for pore fluid

TABLE 1 | Summaries of location, water depth, core length, and SMT depth in each site from the ARA07C and ARA09C Expeditions.

Sample Type	ARAON Mound No	Site	Latitude (°N)	Longitude (°W)	Water Depth (m)	Core Length (m)	SMT Depth (mbsf)	Remark
Pore	Background	ARA09C-St 08	75.7397	169.8545	813	5.29	not reach	Not find GHs and MDACs
Fluid	AM01	ARA09C-St 07	75.7120	169.7947	699	4.51	~3.3	Find MDACs
	AM03	ARA07C-St 14	75.7034	169.7592	653	1.67	~0.9	Find MDACs
		ARA09C-St 16	75.7034	169.7608	662	2.60	< 0.5	Find GHs/MDACs
	AM06	ARA07C-St 13	75.6800	169.7365	610	2.35	~1.3	Find GHs/MDACs
		ARA09C-St 04	75.6799	169.7368	605	2.64	1.2	Find MDACs
		ARA09C-St 06	75.6807	169.7366	609	2.57	< 0.5	Find GHs/MDACs
	AM07	ARA09C-St 12	75.6637	169.7410	582	2.64	~2.1	Find MDACs
Seawater	AM06	ARA09C-St 04	75.6799	169.7367	605	–	–	Bottom water depth: 600 m

-, no data.
MDAC, methane-derived authigenic carbonate; GH, gas hydrate.

and seawater, and then stored at approximately 4°C in the refrigerator until the analyses.

Methane-derived authigenic carbonates were distributed from ~0.2 to ~2.2 meters below the seafloor (mbsf) in the cores during the ARA07C and ARA09C Expeditions (**Table 2**). Some MDACs were observed with several cm-thickness in the split cores (Jin and Shipboard Scientific Party, 2017; Jin and Shipboard Scientific Party, 2019). MDACs were hand-picked in the split cores and collected in plastic bags during these expeditions (**Figure 2**). These samples were stored at approximately 4°C in the refrigerator until the analyses.

Fluid Analyses

The chlorinity (Cl^-) and alkalinity of the pore fluid, hydrate-bound water, and seawater were measured onboard during the ARA07C and ARA09C Expeditions. The Cl^- concentration was measured *via* titration with 0.1 M silver nitrate ($AgNO_3$) and the alkalinity was determined immediately by titration with 0.02 M HCl. The reproducibilities of Cl^- and alkalinity by repeated analyses of the International Association of Physical Sciences of the Oceans (IAPSO) standard seawater were < 2% and < 0.5%, respectively. Sulfate (SO_4^{2-}) in pore fluid and hydrate-bound water from the ARA07C Expedition and the bottom seawater from Site ARA09C-St 04 was analyzed by ion chromatography (IC) at the Korea Basic Science Institute (KBSI; Dionex ICS-1100, Thermo Scientific). IAPSO standard seawater was repeatedly used to verify the analytical quality of the instruments, and the analytical reproducibility was better than 3%. In addition, SO_4^{2-} in pore fluid and hydrate-bound water collected from the ARA09C Expedition was analyzed using the IC at the Kitami Institute of Technology (KIT; 2707 plus Autosampler, 1525 Binary HPLC Pump, and 432 Conductivity Detector, Nihon Waters K.K., Japan). The reproducibility, estimated from repeated analyses of IAPSO standard seawater, was < 3%.

TABLE 2 | Carbon and oxygen isotopic values of MDACs collected during the ARA07C Expedition.

Site	Depth (mbsf)	$\delta^{13}C$ (‰ V-PDB)	$\delta^{18}O$ (‰ V-PDB)
ARA07C-St 13	0.38	-32.7	5.6
	0.44	-31.9	5.2
	0.72	-32.2	5.5
	1.12	-34.4	6.2
	1.16	-25.6	4.6
	1.71	-28.1	5.4
ARA07C-ST 14	0.73	-32.1	5.9
	1.10	-25.6	6.8

Major and minor cations (Na^+, K^+, Mg^{2+}, Ca^{2+}, Sr^{2+}, and H_4SiO_4) were analyzed by inductively coupled plasma-optical emission spectroscopy (Perkin Elmer Optima 8300) at the KBSI. The reproducibility, estimated from repeated analyses of certified reference materials (SLRS-5 and TMDW), was < 5%.

Stable water isotopes (δD and $\delta^{18}O$) of pore fluid, hydrate-bound water, and seawater from the ARA07C and ARA09C Expeditions were determined with a VG Prism stable isotope ratio mass spectrometer (SIRMS) at the KBSI and an off-axis integrated cavity output spectroscopy laser absorption spectrometer (Los Gatos Research (LGR) Liquid Water Isotope Analyzer [LWIA-24d]) at the KIT, respectively. The analytical reproducibilities by the SIRMS and LWIA were ±0.1‰ for $\delta^{18}O$ and ±1‰ for δD, and ±0.2‰ for $\delta^{18}O$ and ±0.6‰ for δD, respectively.

The carbon isotopic composition ($\delta^{13}C_{DIC}$) in the fluid was analyzed with a Finnigan DELTA-Plus mass spectrometer using a Gas-Bench II automated sampler at Oregon State University. The reproducibility was better than 0.07‰, based on the multiple standard measurements. Isotopic values are reported in the conventional δ-notation relative to Vienna Standard Mean Ocean Water (V-SMOW) for hydrogen and oxygen, and Vienna Pee Dee Belemnite (V-PDB) for carbon.

Dissolved strontium in the fluid was separated for isotopic analysis using Sr-Spec columns (Eichrom-Sr resin). Strontium isotopic ratios ($^{87}Sr/^{86}Sr$) were measured using a Neptune multi-collector inductively coupled plasma mass spectrometer (Thermo Finnigan, Bremen, Germany) upgraded with a large dry interface pump at the KBSI. The measured $^{87}Sr/^{86}Sr$ ratios were normalized to $^{86}Sr/^{88}Sr = 0.1194$, and repeated NBS 987 measurements yielded 0.71025 ± 0.00002 ($2\sigma_{mean}$, $n = 24$).

FIGURE 2 | Photographs of methane-derived authigenic carbonate (MDAC) from **(A)** 1.16 mbsf at Site ARA07C-St 13 and **(B)** 1.10 mbsf at Site ARA07C-St 14.

MDAC Analyses

The pretreatment of MDACs from the ARA07C Expedition was performed at the Korea Institute of Geoscience and Mineral Resources (KIGAM). The sample was washed several times using ultrapure distilled water and sonicated for a few minutes to eliminate adhered materials. Then, it was rinsed again with ultrapure distilled water and dried at 60 °C in an oven for 12 h. For $\delta^{13}C$ and $\delta^{18}O$ analyses in MDACs, approximately 5 mg of sample was reacted with 100% H_3PO_4 at 90°C for 5 min, and the evolved CO_2 gas was automatically injected into a VG Prism SIRMS at the KBSI. The analytical reproducibility was better than ±0.1‰ for both $\delta^{13}C$ and $\delta^{18}O$. Isotopic values are reported in the conventional δ-notation relative to V-PDB for carbon and oxygen.

Lipid Biomarkers

The MDAC sample was ultrasonically extracted three times with solvent mixtures (dichloromethane (DCM):methanol (MeOH) (2:1 v/v)). Detailed procedures for lipid biomarker analyses have been previously described by Lee et al. (2018). In short, one-half of the total lipid extract (TLE) was dried over anhydrous Na_2SO_4 and treated with tetrabutylammonium sulfite reagent to remove elemental sulfur. The TLE was chromatographically separated into apolar and polar fractions over an Al_2O_3 column (activated for 2 h at 150°C). The apolar fraction was eluted using hexane:DCM (9:1 v/v), and 40 μL of 5α-androstane (10 μg/ml) was added as an internal standard. The polar fraction was recovered with DCM:MeOH (1:1 v/v) as an eluent and 40 μl of C_{22} 7,16-diol (10 μg/ml) was added as an internal standard. This aliquot was derivatized through silylation, prior to quantification by gas chromatography (GC) and identification with gas chromatography-mass spectrometry (GC-MS). Molecular compounds were determined by comparing their mass spectral fragmentation patterns and retention times with previously published data (Stadnitskaia et al., 2008; Lee et al., 2018). The $\delta^{13}C$ values of lipid compounds are expressed *via* conventional δ-notation relative to V-PDB and the analytical reproducibility is less than ±0.4‰ for all lipid compounds.

RESULTS

Compositional and Isotopic Properties of Fluids

The compositional and isotopic properties of the seawater and pore fluids are represented in **Figure 3** and **Supplementary Table 1**. The Cl^-, Na^+, K^+, $\delta^{18}O$, δD, and $^{87}Sr/^{86}Sr$ values of pore fluids from Sites ARA07C-St 13, ARA07C-St 14, ARA09C-St 04, ARA09C-St 07, ARA09C-St 08, and ARA09C-St 12 are relatively uniform throughout the sampling depth, and these values are generally similar to those of the bottom seawater from Site ARA09C-St 04 (**Figure 3**; **Supplementary Table 1**). However, the downcore profile of SO_4^{2-} from these sites can be classified into two groups. The first group, Site ARA09C-St 08 (reference site), shows a linear decrease from the seawater value (~30 mM) at the top of the sediment to ~24 mM at 5.20 mbsf. In addition, the $\delta^{13}C_{DIC}$ values from this site continuously decrease, ranging from -20.1‰ to -1.3‰ (**Figure 3**; **Supplementary Table 1**). These results imply that Site ARA09C-St 08 does not reach the SMT. In contrast, the downcore profile of SO_4^{2-} in the second group, including Sites ARA07C-St 13, ARA07C-St 14, ARA09C-St 04, ARA09C-St 07, and ARA09C-St 12, exhibits three distinct variations with depth. This profile shows a relatively constant or gradual decrease at shallow depths from the seafloor and then abruptly decreases to the SMT. Below the SMT, it has a relatively constant or a slight decrease (**Figure 3**; **Supplementary Table 1**). The SMT depths of Sites ARA07C-St 13, ARA07C-St 14, ARA09C-St 04, ARA09C-St 07, and ARA09C-St 12 are estimated to be ~1.3 mbsf, ~0.9 mbsf, ~1.2 mbsf, ~3.3 mbsf, and ~2.1 mbsf, respectively (**Figure 3**; **Table 1**). The minimum $\delta^{13}C_{DIC}$ value occurs around the SMT at each site (**Figure 3**; **Supplementary Table 1**).

The downcore profiles of Ca^{2+}, Mg^{2+}, and Sr^{2+} at Sites ARA07C-St 13, ARA07C-St 14, ARA09C-St 04, ARA09C-St 07,

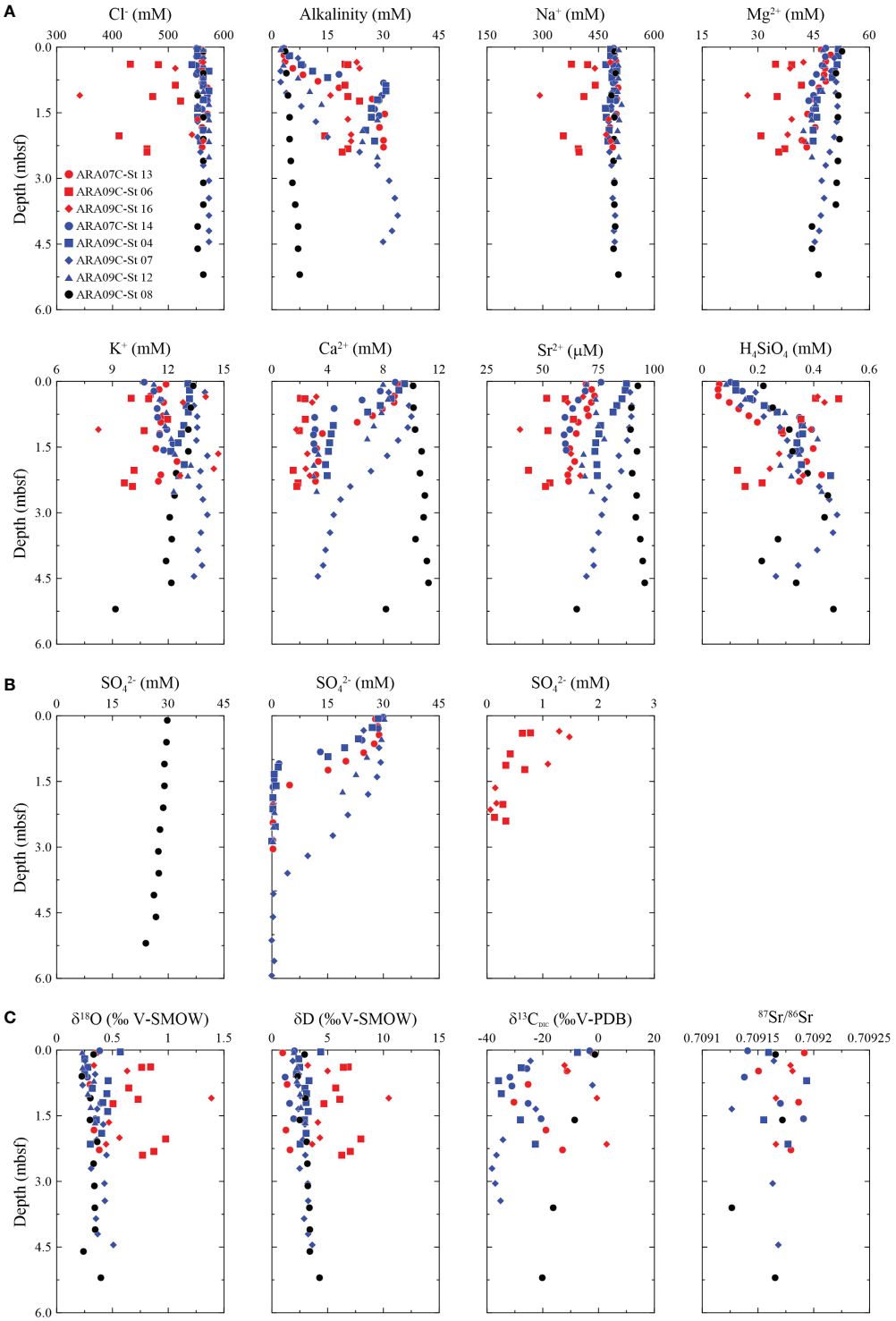

FIGURE 3 | (A) Downcore profiles of Cl^-, alkalinity, Na^+, Mg^{2+}, K^+, Ca^{2+}, Sr^{2+}, and H_4SiO_4 in pore fluids from the ARAON Mounds. **(B)** Downcore profile of SO_4^{2-} in pore fluids from the reference site, non-GH bearing sites, and GH bearing sites in the ARAON Mounds. **(C)** Downcore profiles of $\delta^{18}O$, δD, $\delta^{13}C_{DIC}$, and $^{87}Sr/^{86}Sr$ in pore fluids from the ARAON Mounds. Black color site: reference site without GHs and MDCAs, blue color sites: observation of MDACs, and red color sites: observation of GHs and MDACs.

and ARA09C-St 12 display trends similar to those of SO_4^{2-}. In contrast, the downcore profile of alkalinity oppositely overlaps with that of SO_4^{2-} (**Figure 3**; **Supplementary Table 1**). The H_4SiO_4 concentrations (0.29 ± 0.12 mM, n=64) in all samples from Sites ARA07C-St 13, ARA07C-St 14, ARA09C-St 04, ARA09C-St 07, ARA09C-St 08, and ARA09C-St 12 are higher than that of bottom seawater from Site ARA09C-St 04 (~0.04 mM; **Figure 3**; **Supplementary Table 1**).

Compared to other sites in the ARAON Mounds, chemical compositions (e.g., Cl^-, Na^+, Mg^{2+}, K^+, Ca^{2+}, and Sr^{2+}) have depleted values while stable water isotopes ($\delta^{18}O$ and δD) have enriched values at several intervals of pore fluids from Sites ARA09C-St 06 and ARA09C-St 16 (**Figures 3, 4**; **Supplementary Table 1**). The SO_4^{2-} concentrations at these sites are very low with a maximum value of ~2.0 mM and do not exhibit any distinct trend along the entire core length (**Figure 3**; **Supplementary Table 1**). Alkalinity also shows no trend, and its concentration is greater than ~14 mM at these sites (**Figure 3**; **Supplementary Table 1**). The $\delta^{13}C_{DIC}$ values increase from -12.2‰ at ~0.35 mbsf to 2.9‰ at ~2.15 mbsf of Site ARA09C-St 16 (**Figure 3**; **Supplementary Table 1**), which is a higher value than those of other sites that reach the SMT in the ARAON Mounds. The $^{87}Sr/^{86}Sr$ ratios from Site ARA09C-St 16 are relatively constant (0.70917 ± 0.00001, n=4; **Figure 3**; **Supplementary Table 1**) and are similar to the open seawater (~0.70917; Paytan et al., 1993) and the bottom seawater from Site ARA09C-St 04 (0.70919; **Supplementary Table 1**).

Hydrate-Bound Water

The compositional and isotopic properties of the hydrate-bound waters are represented in **Supplementary Table 1**. Most dissolved chemical compositions in the hydrate-bound waters have lower concentrations than those in pore fluids at the same site. Although the values of $\delta^{18}O$ and δD are limited as we have analyzed one sample from the bottom of Site ARA07C-St 13, they are 2.6‰ and 16.5‰, respectively, which are much higher than those of pore fluids at this site, ranging from 0.3‰ to 0.4‰ and from 0.9‰ and 1.6‰, respectively. However, the $^{87}Sr/^{86}Sr$ ratio in the hydrate-bound water from Site ARA09C-St 16 is 0.70923, which is similar to pore fluids from this site (0.70917 ± 0.00001, n=4; **Figure 3**; **Supplementary Table 1**).

MDACs

The MDACs were observed at Sites ARA07C-St 13 and ARA07C-St 14 during the ARA07C Expedition (**Figure 2**; **Table 2**) and at Sites ARA09C-St 04, ARA09C-St 06, ARA09C-St 07, ARA09C-St 12, and ARA09C-St 16 during the ARA09C Expedition (Jin and Shipboard Scientific Party, 2017; Jin and Shipboard Scientific Party, 2019; Kim et al., 2020). We analyze the $\delta^{13}C$ and $\delta^{18}O$ of MDACs from the ARA07C Expedition. $\delta^{13}C_{MDAC}$ and $\delta^{18}O_{MDAC}$ values vary from -34.4‰ to -25.2‰, and from 4.6‰ to 6.2‰, respectively (**Figure 5**; **Table 2**).

Lipid Biomarker Inventory of MDAC

The MDAC sample includes various lipid components of anaerobic methanotrophs, but there is a lack of biomarkers derived from aerobic methanotrophs. Among the apolar components, the irregular, tail-to-tail linked isoprenoid acyclic C_{20} (2, 6, 11, 15-tetramethylhexadecane or crocetane) and C_{25} (2, 6, 10, 15, 19-pentame-thylicosane, PM) hydrocarbons are present in the MDAC sample. The $\delta^{13}C$ values of the isoprenoid hydrocarbons (i.e., crocetane, PMI) are -119.1‰ and -105.5‰, respectively (**Figure 6**). Similarly, the isoprenoid glycerol diethers archaeol and *sn*-2-hydroxyarchaeol are detected in the polar fractions of MDAC samples with $\delta^{13}C$ values of -104.5‰ to -101.2‰. Another distinct group of detected compounds is non-isoprenoid glycerol diethers (DGDs), tentatively inferred previously as a marker of uncharacterized sulfate reducing bacteria (Werne et al., 2002; Pancost et al., 2011). These compounds (e.g., DGD (If), DGD (IIa), and DGD (IId)) have low $\delta^{13}C$ values in the range of -78.2‰ to -66.1‰ (**Figure 6**).

DISCUSSION

Pore Fluid Source

The dissolved chemical species concentrations and water isotopes ($\delta^{18}O$, δD, and $^{87}Sr/^{86}Sr$) values in pore fluids from Sites ARA07C-St 13, ARA07C-St 14, ARA09C-St 04, ARA09C-St 07, ARA09C-St 08, and ARA09C-St 12 are quite similar to those in the bottom seawater from Site ARA09C-St 04 (**Figure 3**; **Supplementary Table 1**). Moreover, the measured $\delta^{18}O$ and δD values in pore fluids do not have a distinct relationship with each other or with Cl^- concentrations (**Figure 4**). Consequently, the pore fluids at these sites predominantly originate from the overlying ambient seawater in the ARAON Mounds. As H_4SiO_4 and Ca^{2+} concentrations in pore fluid samples from these sites have enriched and depleted values, respectively, compared to the bottom seawater (**Figure 3**; **Supplementary Table 1**), pore fluid properties are likely to be altered within the sediment column by water-rock interactions and by mineral precipitation (Kim et al., 2016; Kim et al., 2022).

In contrast, the downcore profiles of dissolved chemical species and stable water isotopes from Sites ARA09C-St 06 and ARA09C-St 16 show distinctly depleted and enriched excursions at several intervals, respectively, relative to those in pore fluids and seawater from other sites in the ARAON Mounds (**Figures 3** , **4**; **Supplementary Table 1**). In addition, the measured $\delta^{18}O$ and δD values in pore fluids from these sites have a good positive correlation ($R^2 > 0.98$) whereas they show a good negative correlation with Cl^- concentrations ($R^2 > 0.83$) (**Figure 4**). These characteristics are typical when the fluid derived from GH dissociation affects the pore fluid. Indeed, many GHs found *in situ* at Sites ARA09C-St 06 and ARA09C-St 16 during the ARA09C Expedition (Jin and Shipboard Scientific Party, 2019). As the pressure decreases and temperature increases when the cores are retrieved from the sediment column to the deck, GHs in the sediment of

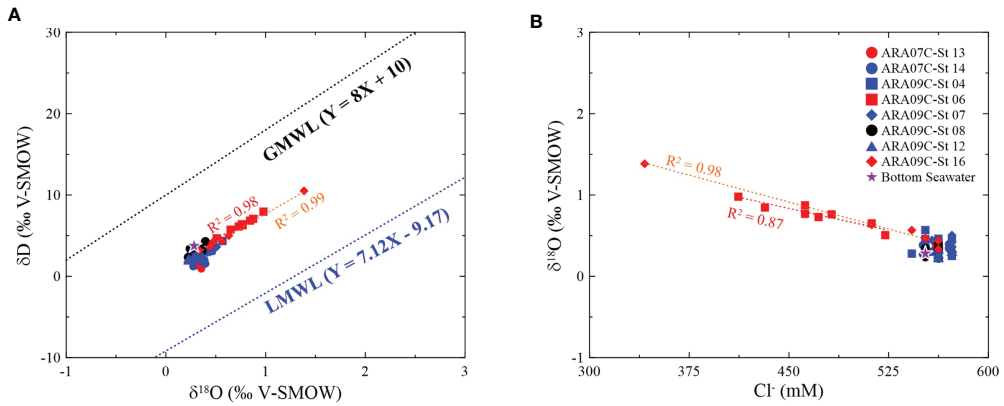

FIGURE 4 | Scatter plots of **(A)** δD versus $\delta^{18}O$ and **(B)** $\delta^{18}O$ versus Cl^- in bottom seawater (violet star; Site ARA09C-St 04) and pore fluids from the ARAON Mounds. The GMWL is the global meteoric water line (**Craig, 1961**), and the LMWL is the local meteoric water line at Inuvik, Canada, by the Global Network of Isotopes in Precipitation (http://www-naweb.iaea.org/napc/ih/IHS_resources_gnip.html). Black color site: reference site without GHs and MDACs, blue color sites: observation of MDACs, and red color sites: observation of GHs and MDACs.

Sites ARA09C-St 06 and ARA09C-St 16 are dissociated and release freshwater into the sediment (e.g., Hesse and Harrison, 1981; Matsumoto and Borowski, 2000; Ussler and Paull, 2001; Hesse, 2003; Torres et al., 2008; Torres et al., 2011). Therefore, the fluid from GH dissociation results in pore fluid freshening with enriched δD and $\delta^{18}O$ values. In addition, because GH dissociation causes the sediment expansion in the core liner during the core retrieving (Kim et al., 2020), ambient seawater can flow sediment in Sites ARA09C-St 06 and ARA09C-St 16. As a result, pore fluid chemistry can be contaminated by the ambient seawater, which interrupts the estimation of the SMT depth of these sites based on the only SO_4^{2-} profile of pore fluids. Overall, the compositional and isotopic properties of pore fluids from Sites ARA09C-St 06 and ARA09C-St 16 have been severely altered by the GH decomposition. We also found an *in situ* GH at the bottom of Site ARA07C-St 13 (core catcher; > 2.35 mbsf), however, the fluid from the GH dissociation cannot significantly influence the pore fluid properties at several intervals of this site, as it does at Sites ARA09C-St 06 and ARA09C-St 16.

Hydrate Saturation

Based on low Cl^- values that are affected by GH dissociation and background Cl^- value in pore fluid that is not affected by GH dissociation, GH saturation (S_h, % of pore space) can be estimated using the following equation (Matsumoto and Borowski, 2000; Ussler and Paull, 2001; Hesse, 2003; Torres et al., 2008; Torres et al., 2011):

$$S_h = \left[\beta\left(C_b - C_s\right)\right] / \left[C_s + \beta\left(C_b - C_s\right)\right] \times 100 \quad \text{(Eq. 1)}$$

where C_b represents the *in situ* background dissolved Cl^- of the water, which in this study is the pore fluid value at 0.35 mbsf from Site ARA09C-St 16 (~563 mM). C_s is the Cl^- measured in the sample after GH dissociation and β is a dimensionless constant that accounts for the density change due to GH dissociation and equals 1.257 (Ussler and Paull, 2001; Malinverno et al., 2008; Torres et al., 2011; Kim et al., 2013).

The estimated S_h values at Sites ARA09C-St 06 and ARA09C-St 16 have ranges of approximately 9-32% (n=8; average=20%) and 2-46% (n=4; average=16%), respectively, which vary widely within < 2.5 m-length core at each site (**Table 3**). These results indicate that the GH is likely to be heterogeneous within the sediment of Sites ARA09C-St 06 and ARA09C-St 16.

Linkage Between SO_4^{2-} Concentration and Methane Flux

The downcore profile of SO_4^{2-} concentration in pore fluids from Site ARA09C-St 08 indicates that this site does not reach the SMT under steady state condition (**Figure 3**). In contrast, these profiles at Sites ARA07C-St 13, ARA07C-St 14, ARA09C-St 04, ARA09C-St 07, and ARA09C-St 12 are concave-up and/or kink type with a minimum SO_4^{2-} concentration of ~0 mM. Since this downcore profile of SO_4^{2-} usually suggests the non-steady state of pore fluid chemistry (Hensen et al., 2003; Henkel et al., 2011), the observed SO_4^{2-} profiles imply that Sites ARA07C-St 13,

TABLE 3 | Gas hydrate saturation (S_h) from Sites ARA09C-St 06 and ARA09C-St 16.

Site	Depth (mbsf)	Cl^- (mM)	S_h (%)
ARA09C-St 06	0.39	432.0	27.6
	0.40	482.3	17.4
	0.87	512.4	11.0
	1.13	472.2	19.5
	1.23	522.5	8.9
	2.03	411.9	31.6
	2.32	462.2	21.5
	2.40	462.2	21.5
ARA09C-St 16	0.48	512.4	11.0
	1.10	341.6	44.9
	1.65	552.6	2.3
	2.00	542.6	4.5

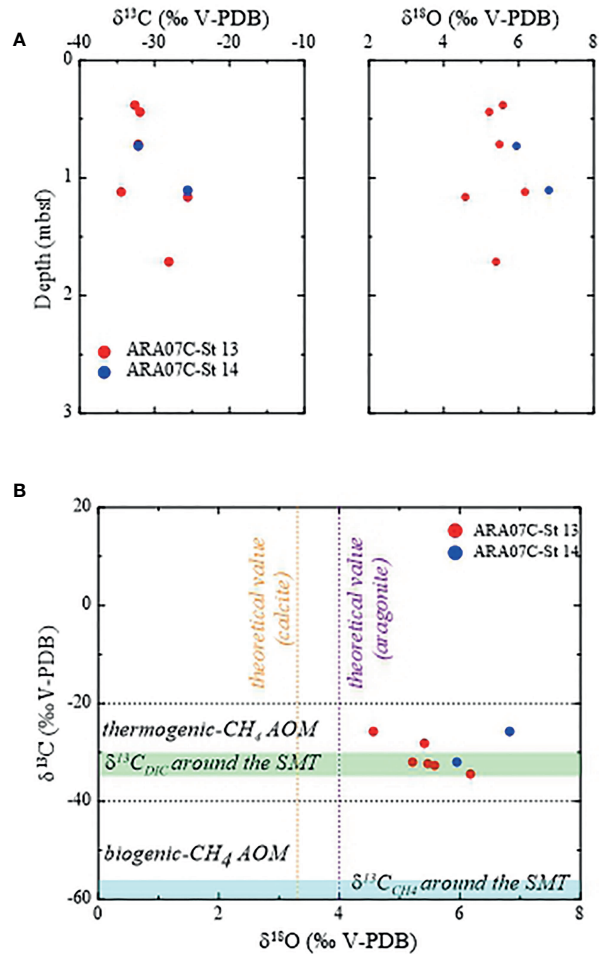

FIGURE 5 | (A) Downcore profiles of $\delta^{13}C$ and $\delta^{18}O$ in MDACs from the ARAON Mounds. **(B)** Scatter plots of $\delta^{13}C$ versus $\delta^{18}O$ in MDACs from the ARAON Mounds. The violet and light orange line are the theoretical $\delta^{18}O_{argonite}$ and $\delta^{18}O_{calcite}$ estimated by the equation of Kim et al. (2007) and Kim and O'Neil (1997), respectively. The upper and lower black lines are boundaries for MDACs incorporated with thermogenic CH_4 and microbial CH_4, respectively (Naehr et al., 2007; Crémière et al., 2016; Crémière et al., 2018). The cyan area and light green area are the ranges of $\delta^{13}C_{CH4}$ (Kim et al., 2020) and $\delta^{13}C_{DIC}$ (this study) around the SMT, respectively. Red closed circles: MDACs from Site ARA07C-St 13 and blue closed circles: MDACs from Site ARA07C-St 14.

ARA07C-St 14, ARA09C-St 04, ARA09C-St 07, and ARA09C-St 12 penetrate the SMT under the non-steady state condition. The non-steady state downcore profiles of SO_4^{2-} have already been documented in many regions such as the Argentine Basin, South China Sea, offshore Namibia, and offshore Svalbard (Niewöhner et al., 1998; Fossing et al., 2000; Hong et al., 2017; Hu et al., 2019), which is attributed to either bioirrigation of macrofauna, seawater intrusion during methane ebullition, mass-transport deposits, or increasing upward methane and fluid flux. Because the bioirrigation of macrofauna has rarely been observed in split sediment cores from Sites ARA07C-St 13, ARA07C-St 14, ARA09C-St 06, and ARA09C-St 16, and methane flares have not been observed at all of ARAON Mounds sites (Jin and Shipboard Scientific Party, 2017; Jin and Shipboard Scientific Party, 2019), bioirrigation of macrofauna and the seawater intrusion associated with methane ebullition have not likely occurred at these mounds. In addition, sediment structures related to mass transport deposits have not been found in the sediment facies and SBP images of ARAON Mounds (Jin and Shipboard Scientific Party, 2017; Jin and Shipboard Scientific Party, 2019; Kim et al., 2021b), implying that large-scale sediment reworking cannot account for the non-steady state of SO_4^{2-}. In contrast, during the ARA07C and ARA09C Expeditions, we found many *in situ* GHs at shallow depths at Sites ARA07C-St 13, ARA09C-St 06, and ARA09C-St 16 (core length < 3 m) (Jin and Shipboard Scientific Party, 2017; Jin and Shipboard Scientific Party, 2019; Kim et al., 2020; Choi et al., 2021). To form the GH near the seafloor in the marine environment, the CH_4 flux from deep-seated sediment to the seafloor through the conduit should be high. Thus, we postulate that the non-steady state shown in the downcore profile of SO_4^{2-} of the ARAON Mounds is linked to the variation in upward CH_4 flux from the deep sediment column. This result is partly consistent with the gas chemistry in the ARAON Mounds (Kim et al., 2020).

Kim et al. (2020) revealed that the CH_4 source originates from thermogenic and microbial, which remarkably changes around the SMT on the basis of gas chemistry in the ARAON Mounds. The thermogenic CH_4 that migrated from deep-seated sediments (> 1 km) toward the seafloor through the faults/fractures alters the shallow gas compositional and isotopic properties below/around the SMT in this mound while the microbial CH_4 mainly impacts the area above/around the SMT (Kim et al., 2020). Since the SO_4^{2-} gradient of pore fluid can be mainly controlled by the upward gas flux in the marine sediment (Borowski et al., 1996; Borowski et al., 1997), its sharp decreasing gradient above the SMT at Sites ARA07C-St 13, ARA07C-St 14, ARA09C-St 04, ARA09C-St 07, and ARA09C-St 12 (**Figure 3**) can be directly attributed to the upward thermogenic CH_4 flux around the SMT. However, this mechanism does not explain a gradually decreasing or non-observed SO_4^{2-} gradient in the shallow sediments of these sites (**Figure 3**). It is likely another process that modifies the fluid chemistry associated with GHs and MDACs within the sediment column.

Impact of MDAC and GH Formation on Fluid Chemistry

The downcore profiles of Ca^{2+}, Mg^{2+}, and Sr^{2+} at Sites ARA07C-St 13, ARA07C-St 14, ARA09C-St 04, ARA09C-St 07, and ARA09C-St 12 generally follow the trend of SO_4^{2-}, with rapidly lower concentrations in the zone showing a linear decrease (**Figure 3**; see *Compositional and Isotopic Properties of Fluids*). These results suggest that intense carbonate precipitation occurs in this zone at each site, as evidenced by the many MDACs found during the ARA07C and ARA09C Expeditions (Jin and Shipboard Scientific Party, 2017; Jin and Shipboard Scientific Party, 2019; Kim et al., 2020). In contrast, an MDAC does not occur above the SMT. Therefore,

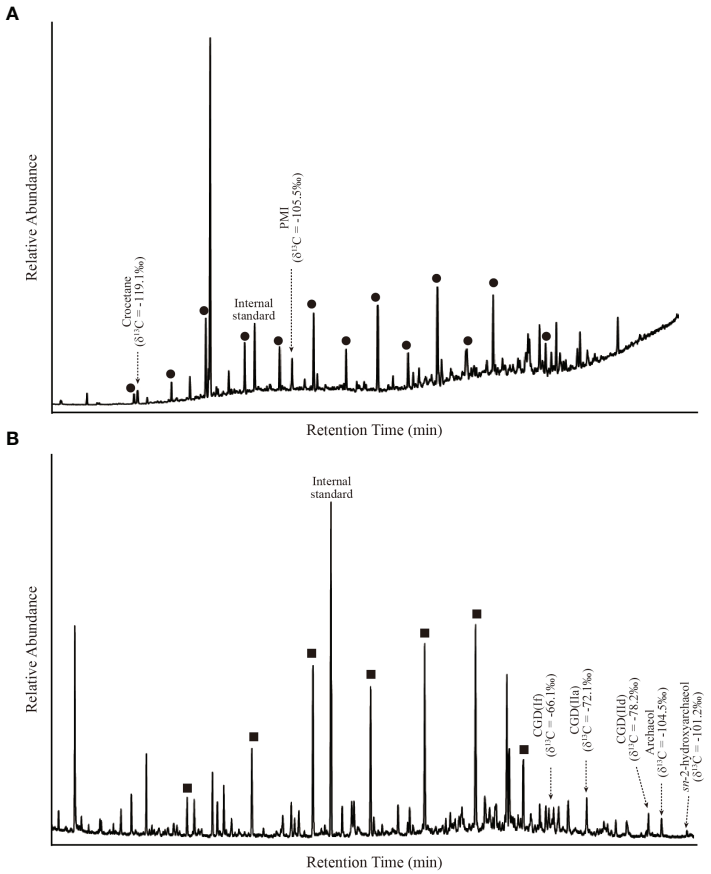

FIGURE 6 | Gas chromatograms of the total lipid extracts from MDAC (1.16 mbsf at Site ARA07C-St 13); **(A)** *n*-alkanes, and **(B)** straight-chain alcohols.

the precipitation of carbonates is likely to be triggered by the increase in alkalinity associated with the AOM.

The carbon isotopes ($\delta^{13}C_{MDAC}$) of MDACs reflect the CH_4 source involved in the AOM reaction. In general, the $\delta^{13}C_{MDAC}$ in association with the thermogenic CH_4 usually ranges from ~-40‰ to -20‰ while it is less than -40‰ by the AOM using microbial CH_4 (Naehr et al., 2007; Crémière et al., 2016; Crémière et al., 2018). The measured $\delta^{13}C_{MDAC}$ values at the ARAON Mounds range from -36.4‰ to -21.9‰ (**Figure 5**), indicating thermogenic CH_4 as a predominant source of MDACs in the ARAON Mounds. This result is consistent with the CH_4 source around/below the present SMT in these mounds (Kim et al., 2020). Under such conditions, specific lipid molecules (e.g., archaeol and *sn*-2-hydroxyarchaeol) preserved within MDAC, can identify the predominance of anaerobic methanotrophs (ANMEs), as well as paleoenvironmental conditions (e.g., methane sources and fluctuation) in association with the AOM reaction during the formation of MDAC (Blumenberg et al., 2004; Elvert and Niemann, 2008; Niemann and Elvert, 2008; Himmler et al., 2015). Typically, microbial communities dominated by ANME-2 at the cold seeps of the northwestern Black Sea contain higher amounts of *sn*-2-hydroxyarchaeol relative to archaeol, whereas the reverse is observed in microbial mats dominated by ANME-1 (Blumenberg et al., 2004). Indeed, the ratio of isotopically depleted *sn-2*-hydroxyarchaeol relative to archaeol can be used to distinguish ANME-1 (0–0.8) from ANME-2 (1.1–5.5), with ANME-3 (2.4) falling within the range of ANME-2 (Niemann et al., 2005; Niemann and Elvert, 2008). The compound ratios (i.e., *sn*-2-hydroxyarchaeol/archaeol) in MDAC from the ARAON Mounds are ~1 (**Figure 6**), implying that ANME-1 is predominantly involved in the AOM reaction to form MDACs using the deep CH_4 sources. The diagnostic archaeal (crocetane, PMI, archaeol, and, *sn*-2-hydroxyarchaeol) and bacterial lipids (DGDs) with strongly depleted ^{13}C in MDAC (**Figure 6**) also support this interpretation.

The formation of MDACs in the ARAON Mounds can drastically alter the physical properties of sediment and flow pathway because it reduces the permeability of sediments and potentially prevents direct flow or retards gas and fluid migration within the sediments (Hovland, 2002; Bahr et al., 2007; Bayon et al., 2009). Similarly, the formation and growth of GHs in the sediment by a high CH_4 flux can modify physical properties and flow pathways (Sassen et al., 1999; Römer et al., 2012; Sultan et al., 2014). Therefore, we postulate that MDACs and GHs observed widespread in the ARAON Mounds are likely to prevent

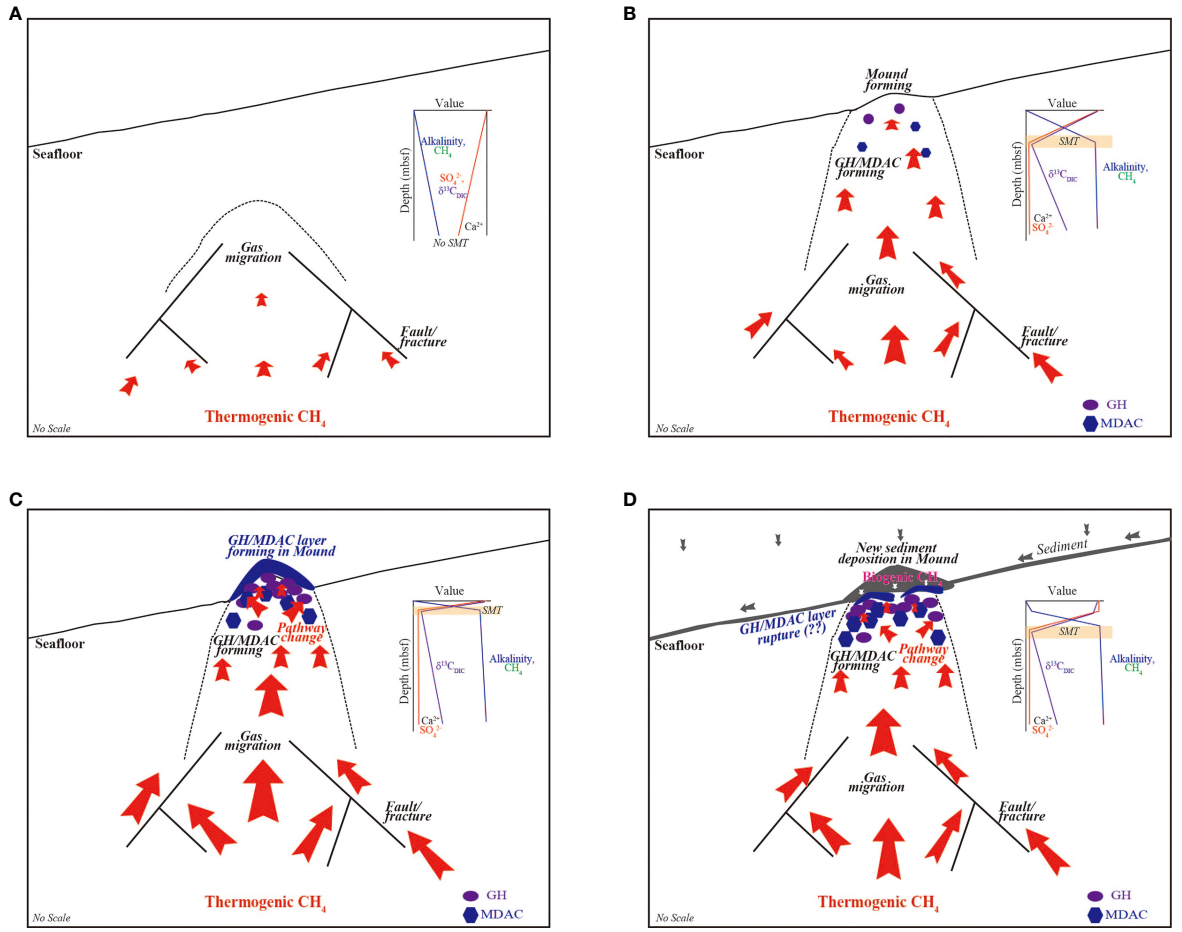

FIGURE 7 | Schematic diagram illustrating the change of seafloor morphology, fluid and gas migration, fluid chemistry (SO_4^{2-}, alkalinity, Ca^{2+}, CH_4, and $\delta^{13}C_{DIC}$), and MDACs and GHs production in the ARAON Mounds in association with the CH_4 flux; **(A)** beginning of the upward CH_4 flux from the deep sediment, **(B)** mound formation on the seafloor and beginning of GH and MDAC production in the sediment column under high upward CH_4 flux, **(C)** GH and MDAC production in the seafloor and flow pathway change under a high upward CH_4 flux, and **(D)** new sediment deposition at the mound and/or GH and MDAC production under a high upward CH_4 flux.

or interrupt the upward migration of gas and fluid in the sediment column (**Figure 7**). Given that the fluid coupled with gas continuously migrates through the sediment column, the downcore profile of SO_4^{2-} reaches steady state condition and the CH_4 source should be steadily changed from the seafloor to deep-seated sediment with the CH_4 flux (**Figures 7A–C**). Otherwise, the upward gas and fluid are blocked or redirected by MDACs and GHs within the sediment column, and then sediment is continuously deposited over them within a short time scale. The gas and pore fluid chemistry above these deposits are mainly controlled by ambient seawater and by (bio)geochemical reactions (e.g., organic matter degradation by sulfate reduction, microbial methanogenesis) associated with the microbial activity to degrade the organic matter rather than by the upward CH_4 flux (**Figure 7D**). As a result, the chemical zone is entirely separated between the below and above deposition of the MDACs and GHs (**Figure 7D**).

Influence of Methane Flux and GH Dissociation on MDAC Chemistry

The $\delta^{18}O$ signature of carbonates can inform the oxygen isotopic composition of the fluid when the carbonate precipitates (e.g., Greinert et al., 2001; Naehr et al., 2007). Assuming that aragonite and carbonated formed in isotopic equilibrium with ambient bottom seawater at the temperature and $\delta^{18}O$ value of the ARAON Mounds, respectively, the theoretical $\delta^{18}O_{aragonite}$ and $\delta^{18}O_{carbonate}$ values can be estimated by these equations (Kim and O'Neil, 1997; Kim et al., 2007);

$$1000\ln\alpha_{aragonite\text{-}seawater} = 17.88\times\frac{10^3}{T}(\text{Kelvin}) - 31.14 \quad \text{(Eq. 2)}$$

$$1000\ln\alpha_{calcite\text{-}seawater} = 18.03\times\frac{10^3}{T}(\text{Kelvin}) - 32.42 \quad \text{(Eq. 3)}$$

The temperature and $\delta^{18}O$ value of the present bottom seawater from Site ARA09C-St 04, as measured during the ARA09C Expedition, are 0.8°C (Jin and Shipboard Scientific Party, 2019) and 0.3‰ (V-SMOW; **Supplementary Table 1**), respectively. Thus, the theoretical $\delta^{18}O$ of aragonite and carbonate is ~4.0‰ (V-PDB) and ~3.3‰ (V-PDB), respectively. All analyzed $\delta^{18}O_{MDAC}$ values from Sites ARA07C-St 13 and ARA07C-St 14 are higher than these calculated equilibrium values (**Figure 5**; **Table 2**), suggesting the incorporation of enriched ^{18}O fluid during MDAC precipitation. The enriched ^{18}O fluid may originate from either clay mineral dehydration, opal diagenesis, or GH dissociation (Hesse and Harrison, 1981; Kastner et al., 1991; Ussler and Paull, 1995; Hesse, 2003; Kim et al., 2013; Kim et al., 2021a). In general, the $^{87}Sr/^{86}Sr$ ratio tends to be lower than that of the ambient present seawater by clay dehydration, and the $\delta^{18}O$ value increases with a relatively constant δD value by opal diagenesis (Kastner et al., 1991; Kim et al., 2013; Kim et al., 2021a). Since most $^{87}Sr/^{86}Sr$ ratios in pore fluids are similar to the present bottom seawater of ARA09C-St 04 and the values of $\delta^{18}O$ and δD are relatively constant in the non-GH-bearing intervals, irrespective of sampling depth **(Figures 3, 4; Supplementary Table 1**), we excluded clay mineral dehydration and opal diagenesis as the primary sources for enriched ^{18}O fluid in the ARAON Mounds. Instead, it is reasonable that the ^{18}O-enrichment of MDACs can be attributed to fluids derived from GH dissociation in relation to climate change through geological time (Greinert et al., 2001; Naehr et al., 2007), as indicated by the occurrences of shallow GHs around MDACs at Sites ARA07-St 13, ARA09C-St 06, and ARA09C-St 16 (**Figures 1**, **2**; **Tables 1**, **2**; **Supplementary Table 1**).

SUMMARY AND IMPLICATIONS

The compositional and isotopic properties (e.g., Cl^-, Na^+, δD, $\delta^{18}O$, and $^{87}Sr/^{86}Sr$) of pore fluids from Sites ARA07C-St 13, ARA07C-St 14, ARA09C-St 04, ARA09C-St 07, ARA09C-St 08, and ARA09C-St 12 are similar to those of bottom seawater from Site ARA09C-St 04, indicating that the source of pore fluid is mainly derived from the ambient seawater in the ARAON Mounds. In contrast, pore fluids from Sites ARA09C-St 06 and ARA09C-St 16, where many *in situ* GHs are found, have low Cl^- concentrations with high δD and $\delta^{18}O$ values, which are typical features of fluids affected by GH dissociation. At these sites, the SO_4^{2-} downcore profiles have no distinct trend with higher $\delta^{13}C_{DIC}$ values (-12.2‰ to 2.9‰ at Site ARA09C-St 16) compared to other sites and prevent the estimation of the SMT, which also supports the impact of GH dissociation. Interestingly pore fluids from Site ARA07C-St 13 do not have typical characteristics that are affected by GH dissociation while they show similar properties to those of the bottom seawater from Site ARA09C-St 04, even though GHs were found at the end of the sediment core.

The SO_4^{2-} downcore profile from Site ARA09C-St 08 does not reach the SMT (minimum SO_4^{2-} concentration = ~25 mM) under a steady-state condition with a linearly decreasing trend. In contrast, these profiles from Sites ARA07C-St 13, ARA07C-St 14, ARA09C-St 04, ARA09C-St 07, and ARA09C-St 12 are concave-up and/or kink type, with a minimum SO_4^{2-} concentration of ~0 mM, indicating the penetration of the SMT under the non-steady state condition. Many *in situ* MDACs and GHs have been widely found in the sediment, thus, the observed trend of the SO_4^{2-} downcore profile is strongly associated with them. When the gas and fluid continuously flow upward, these byproducts prevent and/or at least severely retard as well as redirect their flow pathways through the sediments because the physical properties of the sediment and fluid pathways are remarkably changed by them. As a result, the exchange of dissolved species does not take place smoothly within the sediment column between the bearing and non-bearing GH and MDAC intervals, which leads to the separation of chemical zones between them. Hence, the downcore profiles of SO_4^{2-} and other dissolved ions (e.g., Ca^{2+}, Mg^{2+}, and alkalinity) have concave-up and/or kink type under the non-steady state condition. Overall, the pore fluid chemistry in the ARAON Mounds exhibits spatiotemporal variations in response to the CH_4 flux as well as the existence of GH and MDACs.

The $\delta^{13}C_{MDAC}$ values of all MDACs from Sites ARA07C-St 13 and ARA07C-St 14 are higher than -40‰, and $\delta^{18}O_{MDAC}$ values are also higher than the theoretical equilibrium values (~4.0‰ for aragonite and ~3.3‰ for calcite, respectively) on the basis of the temperature and $\delta^{18}O$ value of the bottom seawater from Site ARA09C-St 04. These results imply that thermogenic CH_4 migrates from the deeper sediment and that the ^{18}O-enriched fluid derived from GH dissociation incorporates to precipitate carbonate.

It is expected that rapid global warming will continuously amplify in the future (Schuur et al., 2015; Kim et al., 2021a). We can also predict that the seafloor morphology and regional hydrology including the formation of GHs and MDACs of the ARAON Mounds as well as other regions of the Arctic Ocean, will rapidly change in association with future climate change. The present information of fluids and MDACs observed in the ARAON Mounds can provide some clues to predict these changes at these mounds and in the Arctic Ocean in response to future climate change. To precisely understand and predict these changes due to future climate change, more studies targeting methane seepage and its role in the Arctic Ocean are needed.

DATA AVAILABILITY STATEMENT

The original contributions presented in the study are included in the article/**Supplementary Material**. Further inquiries can be directed to the corresponding author.

AUTHOR CONTRIBUTIONS

J-HK designed and coordinated the study, analyzed the samples, interpreted the data, and led the writing of the

manuscript. M-HP, D-HL, HM, AH, J-SR, YS and SP analyzed the samples, wrote, and reviewed the manuscript. Y-KJ, M-HK, MK, and J-HK conducted the survey, wrote, and reviewed the draft. JH, KJ, YS, and MC interpreted the data, wrote, and reviewed the manuscript. All authors assisted with interpretation and contributed to the writing of the manuscript.

FUNDING

This study was funded by Korea Ministry of Science and ICT (GP2020-006 and GP2021-009), by the Korea Ministry of Oceans and Fisheries (20210632), and by Korea Ministry of Trade, Industry and Energy (Project No. 20212010200010).

ACKNOWLEDGMENTS

We would like to thank the captain and crew of the *IBRV* ARAON for their help at sea. We also gratefully acknowledge the comments from Jörn Peckmann and reviewers, which improved this manuscript.

SUPPLEMENTARY MATERIAL

The Supplementary Material for this article can be found online at: https://www.frontiersin.org/articles/10.3389/fmars.2022.944841/full#supplementary-material

REFERENCES

Aloisi, G., Pierre, C., Rouchy, J.-M., Foucher, J.-P. and Woodside, J. (2000). Methane-Related Authigenic Carbonates of Eastern Mediterranean Sea Mud Volcanoes and Their Possible Relation to Gas Hydrate Destabilisation. *Earth Planet. Sci. Lett.* 184, 321–338. doi: 10.1016/S0012-821X(00)00322-8

Argentino, C., Waghorn, K. A., Vadakkepuliyambatta, S., Polteau, S., Bünz, S. and Panieri, G. (2021). Dynamic and History of Methane Seepage in the SW Barents Sea: New Insights From Leirdjupet Fault Complex. *Sci. Rep.* 11, 4373. doi: 10.1038/s41598-021-83542-0

Bahr, A., Pape, T., Bohrmann, G., Mazzini, A., Haeckel, M., Reitz, A., et al. (2007). Authigenic Carbonate Precipitates From the NE Black Sea: A Mineralogical, Geochemical, and Lipid Biomarker Study. *Int. J. Earth Sci.* 98, 677–695. doi: 10.1007/s00531-007-0264-1

Barnes, R. O. and Goldberg, E. D. (1976). Methane Production and Consumption in Anoxic Marine Sediments. *Geology* 4, 297–300. doi: 10.1130/0091-7613(1976)4<297:MPACIA>2.0.CO;2

Bayon, G., Henderson, G. M. and Bohn, M. (2009). U-Th Stratigraphy of a Cold Seep Carbonate Crust. *Chem. Geol.* 260, 47–56. doi: 10.1016/j.chemgeo.2008.11.020

Blumenberg, M., Seifert, R., Reitner, J., Pape, T. and Michaelis, W. (2004). Membrane Lipid Patterns Typify Distinct Anaerobic Methanotrophic Consortia. *PNAS* 101, 11111–11116. doi: 10.1073/pnas.0401188101

Boetius, A., Ravenschlag, K., Schubert, C. J., Rickert, D., Widdel, F., Gieseke, A., et al. (2000). A Marine Microbial Consortium Apparently Mediating Anaerobic Oxidation of Methane. *Nature* 407, 623–626. doi: 10.1038/35036572

Boetius, A. and Wenzhöfer, F. (2013). Seafloor Oxygen Consumption Fuelled by Methane From Cold Seeps. *Nat. Geosci.* 6, 725–734. doi: 10.1038/ngeo1926

Borowski, W. S., Paull, C. K. and Ussler, W.III. (1996). Marine Pore-Water Sulfate Profiles Indicate *in Situ* Methane Flux From Underlying Gas Hydrate. *Geology* 24, 655–658. doi: 10.1130/0091-7613(1996)024<0655:MPWSPI>2.3.CO;2

Borowski, W. S., Paull, C. K. and Ussler, W.III. (1997). Carbon Cycling Within the Upper Methanogenic Zone of Continental Rise Sediments: An Example From the Methane-Rich Sediments Overlying the Blake Ridge Gas Hydrate Deposits. *Mar. Chem.* 57, 299–311. doi: 10.1016/S0304-4203(97)00019-4

Buerk, D., Klaucke, I., Sahling, H. and Weinrebe, W. (2010). Morpho-Acoustic Variability of Cold Seeps on the Continental Slope Offshore Nicaragua: Results of Fluid Flow Interaction With Sedimentary Processes. *Mar. Geol.* 275, 53–65. doi: 10.1016/j.margeo.2010.04.007

Campbell, K. A. (2006). Hydrocarbon Seep and Hydrothermal Vent Paleoenvironments and Paleontology: Past Developments and Future Research Directions. *Palaeogeogr. Palaeoclimatol. Palaeoecol.* 232, 362–407. doi: 10.1016/j.palaeo.2005.06.018

Chapman, R., Pohlman, J., Coffin, R., Chanton, J. and Lapham, L. (2004). Thermogenic Gas Hydrates in the Northern Cascadia Margin. *EOS (Transactions. Am. Geophysical. Union).* 85, 361–368. doi: 10.1029/2004EO380001

Choi, W., Lee, J., Kim, Y.-G., Kim, H., Rhee, T. S., Jin, Y. K., et al. (2021). The Impact of the Abnormal Salinity Enrichment in Pore Water on the Thermodynamic Stability of Marine Natural Gas Hydrates in the Arctic Region. *Sci. Total. Environ.* 799, 149357. doi: 10.1016/j.scitotenv.2021.149357

Craig, H. (1961). Isotopic Variation in Meteoric Waters. *Science* 133, 1702–1703. doi: 10.1126/science.133.3465.1702

Crémière, A., Chand, S., Sahy, D., Thorsnes, T., Martma, T., Noble, S. R., et al. (2018). Structural Controls on Seepage of Thermogenic and Microbial Methane Since the Last Glacial Maximum in the Harstad Basin, Southwest Barents Sea. *Mar. Petrol. Geol.* 98, 569–581. doi: 10.1016/j.marpetgeo.2018.07.010

Crémière, A., Lepland, A., Chand, S., Sahy, D., Kirsimäe, K., Bau, M., et al. (2016). Fluid Source and Methane-Related Diagenetic Processes Recorded in Cold Seep Carbonates From the Alvheim Channel, Central North Sea. *Chem. Geol.* 432, 16–33. doi: 10.1016/j.chemgeo.2016.03.019

Elvert, M. and Niemann, H. (2008). Occurrence of Unusual Steroids and Hopanoids Derived From Aerobic Methanotrophs at an Active Marine Mud Volcano. *Org. Geochem.* 39, 167–177. doi: 10.1016/j.orggeochem.2007.11.006

Fossing, H., Ferdelman, T. G. and Berg, P. (2000). Sulfate Reduction and Methane Oxidation in Continental Margin Sediments Influenced by Irrigation (South-East Atlantic Off Namibia). *Geochim. Cosmochim. Acta* 64, 897–910. doi: 10.1016/S0016-7037(99)00349-X

Grantz, A., Clark, D. L., Phillips, R. L., Srivastava, S. P., Blome, C. D., Gray, L. B., et al. (1998). Phanerozoic Stratigraphy of Northwind Ridge, Magnetic Anomalies in the Canada Basin, and the Geometry and Timing of Rifting in the Amerasia Basin, Arctic Ocean. *Geol. Soc Am. Bull.* 110, 801–820. doi: 10.1130/0016-7606(1998)110<0801:PSONRM>2.3.CO;2

Greinert, J., Bohrmann, G. and Suess, E. (2001). "Gas Hydrate-Associated Carbonates and Methane-Venting at Hydrate Ridge: Classification, Distribution, and Origin of Authigenic Lithologies," in *Natural Gas Hydrates: Occurrence, Distribution, and Detection*. Eds. Paull, C. K. and Dillon, W. P. (Washington, D.C: American Geophysical Union), 99–113.

Henkel, S., Schwenk, T., Hanebuth, T. J. J., Strasser, M., Riedinger, N., Formolo, M., et al. (2011). "Pore Water Geochemistry as a Tool for Identifying and Dating Recent Mass-Transport Deposits," in *Submarine Mass Movements and Their Consequences*. Eds. Yamada, Y., Kawamura, K., Ikehara, K., Ogawa, Y., Urgeles, R., Mosher, D., Chaytor, J. and Strasser, M. (Dordrecht, Heidelberg, London, New York: Springer), 87–97.

Hensen, C., Zabel, M., Pfeifer, K., Schwenk, T., Kasten, S., Riedinger, N., et al. (2003). Control of Sulfate Pore-Water Profiles by Sedimentary Events and the Significance of Anaerobic Oxidation of Methane for the Burial of Sulfur in Marine Sediments. *Geochim. Cosmochim. Acta* 67, 2631–2647. doi: 10.1016/S0016-7037(03)00199-6

Hesse, R. (2003). Pore Water Anomalies of Submarine Gas-Hydrate Zones as Tool to Assess Hydrate Abundance and Distribution in the Subsurface: What Have We Learned in the Past Decade? *Earth-Sci. Rev.* 61, 149–179. doi: 10.1016/S0012-8252(02)00117-4

Hesse, R. and Harrison, W. E. (1981). Gas Hydrates (Clathrates) Causing Pore-Water Freshening and Oxygen Isotope Fractionation in Deep-Water Sedimentary Sections of Terrigenous Continental Margins. *Earth Planet. Sci. Lett.* 55, 453–462. doi: 10.1016/0012-821X(81)90172-2

Himmler, T., Birgel, D., Bayon, G., Pape, T., Ge, L., Bohrmann, G., et al. (2015). Formation of Seep Carbonates Along the Makran Convergent Margin, Northern Arabian Sea and a Molecular and Isotopic Approach to Constrain the Carbon Isotopic Composition of Parent Methane. *Chem. Geol.* 415, 102–117. doi: 10.1016/j.chemgeo.2015.09.016

Himmler, T., Brinkmann, F., Bohrmann, G. and Peckmann, J. (2011). Corrosion Patterns of Seep-Carbonates From the Eastern Mediterranean Sea. *Terra. Nova.* 23, 206–212. doi: 10.1111/j.1365-3121.2011.01000.x

Hong, W. L., Torres, M. E., Carroll, J., Cremiere, A., Panieri, G., Yao, H., et al. (2017). Seepage From an Arctic Shallow Marine Gas Hydrate Reservoir is Insensitive to Momentary Ocean Warming. *Nat. Commun.* 8, 5745. doi: 10.1038/ncomms15745

Hovland, M. (2002). On the Self-Sealing Nature of Marine Seeps. *Cont. Shelf. Res.* 22, 2387–2394. doi: 10.1016/S0278-4343(02)00063-8

Hu, Y., Luo, M., Liang, Q., Chen, L., Feng, D., Yang, S., et al. (2019). Pore Fluid Compositions and Inferred Fluid Flow Patterns at the Haima Cold Seeps of the South China Sea. *Mar. Petrol. Geol.* 103, 29–40. doi: 10.1016/j.marpetgeo.2019.01.007

Jakobsson, M. (2002). Hypsometry and Volume of the Arctic Ocean and its Constituent Seas. *Geochem. Geophys. Geosyst.* 3, 1–18. doi: 10.1029/2001GC000302

Jin, Y. K.Shipboard Scientific Party (2017). *ARA07C Cruise Report: 2016 Korea-Russia-Germany East Siberian Sea Research Program* (Incheon: Korea Polar Research Institute).

Jin, Y. K.Shipboard Scientific Party (2019). *ARA09C Cruise Report: 2018 Korea-Russia-Japan East Siberian/Chukchi Sea Research Program* (Incheon: Korea Polar Research Institute).

Judd, A. G. and Hovland, M. (2007). *Seabed Fluid Flow* (New York: Cambridge University Press).

Judd, A. G., Hovland, M., Dimitrov, L. I., Garcia, G. S. and Jukes, V. (2002). The Geological Methane Budget at Continental Margins and its Influence on Climate Change. *Geofluids* 2, 109–126. doi: 10.1046/j.1468-8123.2002.00027.x

Kastner, M., Elderfield, H. and Martin, J. B. (1991). Fluids in Convergent Margins - What Do We Know About Their Composition, Origin, Role in Diagenesis and Importance for Oceanic Chemical Fluxes. *Philos. Trans. R. Soc A.* 335, 243-259. doi: 10.1098/rsta.1991.0045.

Kim, J.-H., Hachikubo, A., Kida, M., Minami, H., Lee, D.-H., Jin, Y. K., et al. (2020). Upwarding Gas Source and Postgenetic Processes in the Shallow Sediments From the ARAON Mounds, Chukchi Sea. *J. Nat. Gas. Sci. Eng.* 76, 103223. doi: 10.1016/j.jngse.2020.103223

Kim, J.-H., Hong, W.-L., Torres, M. E., Ryu, J.-S., Kang, M.-H., Han, D., et al. (2021a). A Pulse of Meteoric Subsurface Fluid Discharging Into the Chukchi Sea During the Early Holocene Thermal Maximum (EHTM). *Geochem. Geophys. Geosyst.* 22, e2021GC009750. doi: 10.1029/2021GC009750

Kim, J.-H., Ryu, J. S., Hong, W.-L., Jang, K., Joo, Y. J., Lemarchand, D., et al. (2022). Assessing the Impact of Freshwater Discharge on the Fluid Chemistry in the Svalbard Fjords. *Sci. Total. Environ.* 835, 155516. doi: 10.1016/j.scitotenv.2022.155516

Kim, J.-H., Torres, M. E., Haley, B. A., Ryu, J. S., Park, M. H., Hong, W.-L., et al. (2016). Marine Silicate Weathering in the Anoxic Sediment of the Ulleung Basin: Evidence and Consequences. *Geochem. Geophys. Geosyst.* 17, 3437–3453. doi: 10.1002/2016GC006356

Kim, J.-H., Torres, M. E., Hong, W.-L., Choi, J., Riedel, M., Bahk, J.-J., et al. (2013). Pore Fluid Chemistry From the Second Gas Hydrate Drilling Expedition in the Ulleung Basin (UBGH2): Source, Mechanisms and Consequences of Fluid Freshening in the Central Part of the Ulleung Basin, *East Sea. Mar. Petrol. Geol.* 47, 99–112. doi: 10.1016/j.marpetgeo.2012.12.011

Kim, S., Polyak, L., Joe, Y. J., Nissem, F., Kim, H. J., Cho, Y., et al. (2021b). Seismostratigraphic and Geomorphic Evidence for the Glacial History of the Northwestern Chukchi Margin, Arctic Ocean. *J. Geophys. Res. Earth Surf.* 126, e2020JF006030. doi: 10.1029/2020JF006030

Kim, S. T. and O'Neil, J. R. (1997). Equilibrium and Nonequilibrium Oxygen Isotope Effects in Synthetic Carbonates. *Geochim. Cosmochim. Acta* 61, 3461–3475. doi: 10.1016/S0016-7037(97)00169-5

Kim, S.-T., O'Neil, J. R., Hillaire-Marcel, C. and Mucci, A. (2007). Oxygen Isotope Fractionation Between Synthetic Aragonite and Water: Influence of Temperature and Mg^{2+} Concentration. *Geochem. Cosmochim. Acta* 71, 4704–4715. doi: 10.1016/j.gca.2007.04.019

Koch, S., Berndt, C., Bialas, J., Haeckel, M., Crutchley, G., Papenberg, C., et al. (2015). Gas-Controlled Seafloor Doming. *Geology* 43, 571–574. doi: 10.1130/G36596.1

Lee, D.-H., Kim, J.-H., Lee, Y. M., Kim, J.-H., Jin, Y. K., Paull, C., et al. (2021). Geochemical and Microbial Signatures of Siboglinid Tubeworm Habitats at an Active Mud Volcano in the Canadian Beaufort Sea. *Front. Mar. Sci.* 8. doi: 10.3389/fmars.2021.656171

Lee, D. H., Kim, J.-H., Lee, Y. M., Stadnitskaia, A., Jin, Y. K., Niemann, H., et al. (2018). Biogeochemical Evidence of Anaerobic Methane Oxidation on Active Submarine Mud Volcanoes on the Continental Slope of the Canadian Beaufort Sea. *Biogeosciences* 15, 7419–7433. doi: 10.5194/bg-15-7419-2018

Luff, R., Wallmann, K., and Aloisi, G. (2004). Numerical modeling of carbonate crust formation at cold vent sites: significance for fluid and methane budgets and chemosynthetic biological communities. *Earth Planet. Sci. Lett.* 221, 337-353. doi: 10.1016/S0012-821X(04)00107-4

Malinverno, A., Kastner, M., Torres, M. E. and Wortmann, U. G. (2008). Gas Hydrate Occurrence in a Transect Across the Cascadia Margin From Pore Water Chlorinity and Downhill Geophysical Logs (IODP 311). *J. Geophys. Res.* 113, B08103. doi: 10.1029/2008JB005702

Matsumoto, R. and Borowski, W. S. (2000). "Gas Hydrate Estimates From Newly Determined Oxygen Isotopic Fractionation ($\alpha_{GH\text{-}IW}$) and $\delta^{18}O$ Anomalies of the Interstitial Waters: Leg 164, Blake Ridge," in *Proceedings of the Ocean Drilling Program Scientific Results*, vol. 164 . Eds. Paull, C. K., Matsumoto, R., Wallace, P. J. and Dillon, W. P. (College Station, TX: Ocean Drilling Program), 59–66.

Naehr, T. H., Eichhubl, P., Orphan, V. J., Hovland, M., Paull, C. K., Ussler, W., III, et al. (2007). Authigenic Carbonate Formation at Hydrocarbon Seeps in Continental Margin Sediments: A Comparative Study. *Deep-Sea. Res. II.: Top. Stud. Oceanogr.* 54, 1268–1291. doi: 10.1016/j.dsr2.2007.04.010.

Niemann, H. and Elvert, M. (2008). Diagnostic Lipid Biomarker and Stable Carbon Isotope Signatures of Microbial Communities Mediating the Anaerobic Oxidation of Methane With Sulphate. *Org. Geochem.* 39, 1668–1677. doi: 10.1016/j.orggeochem.2007.11.003

Niemann, H., Elvert, M., Hovland, M., Orcutt, B., Judd, A., Suck, I., et al. (2005). Methane Emission and Consumption at a North Sea Gas Seep (Tommeliten Area). *Biogeosciences* 2, 335–351. doi: 10.5194/bg-2-335-2005

Niewöhner, C., Hensen, C., Kasten, S., Zabel, M. and Schulz, H. D. (1998). Deep Sulfate Reduction Completely Mediated by Anaerobic Methane Oxidation in Sediments of the Upwelling Area Off Namibia. *Geochim. Cosmochim. Acta* 62, 455–464. doi: 10.1016/S0016-7037(98)00055-6

Pancost, R. D., McClymont, E. L., Bingham, E. M., Roberts, Z., Charman, D. J., Hornibrook, E. R. C., et al. (2011). Archaeol as a Methanogen Biomarker in Ombrotrophic Bogs. *Org. Geochem.* 42, 1279–1287. doi: 10.1016/j.orggeochem.2011.07.003

Paull, C. K., Hecker, B., Commeau, R., Freeman-Lynde, R. P., Neumann, C., Corso, W. P., et al. (1984). Biological Communities at the Florida Escarpment Resemble Hydrothermal Vent Taxa. *Science* 226, 965–967. doi: 10.1126/science.226.4677.965

Paull, C. K., Normark, W. R., Ussler, W., III., Caress, D. W. and Keaten, R. (2008). Association Among Active Seafloor Deformation, Mound Formation, and Gas Hydrate Growth and Accumulation Within the Seafloor of the Santa Monica Basin, Offshore California. *Mar. Geol.* 250, 258–275. doi: 10.1016/j.margeo.2008.01.011

Paytan, A., Kastner, M., Martin, E. E., Macdougall, J. D. and Herbert, T. (1993). Marine Barite as a Monitor of Seawater Strontium Isotope Composition. *Nature* 366, 445–449. doi: 10.1038/366445a0

Reeburgh, W. S. (1976). Methane Consumption in Cariaco Trench Waters and Sediments. *Earth Planet. Sci. Lett.* 28, 337–344. doi: 10.1016/0012-821X(76)90195-3

Römer, M., Sahling, H., Pape, T., Bahr, A., Feseker, T., Wintersteller, P., et al. (2012). Geological Control and Quantity of Methane Ebullition From a High-Flux Seep Area in the Black Sea-The Kerch Seep Area. *Mar. Geol.* 319-322, 57–74. doi: 10.1016/j.margeo.2012.07.005

Römer, M., Sahling, H., Pape, T., Ferreira, C. D., Wenzhofer, F., Boetius, A., et al. (2014). Methane Fluxes and Carbonate Deposits at a Cold Seep Area of the Central Nile Deep Sea Fan, Eastern Mediterranean Sea. *Mar. Geol.* 347, 27–42. doi: 10.1016/j.margeo.2013.10.011

Sahling, H., Rickert, D., Lee, R. W., Linke, P. and Suess, E. (2002). Macrofaunal Community Structure and Sulfide Flux at Gas Hydrate Deposits From the

Cascadia Convergent Margin, NE Pacific. *Mar. Ecol. Prog. Ser.* 231, 121–138. doi: 10.3354/meps231121

Sassen, R., Joye, S., Sweet, S. T., DeFreitas, D. A., Milkov, A. V. and MacDonald, I. R. (1999). Thermogenic Gas Hydrates and Hydrocarbon Gases in Complex Chemosynthetic Communities, Gulf of Mexico Continental Slope. *Org. Geochem.* 30, 485–497. doi: 10.1016/S0146-6380(99)00050-9

Sauer, S., Hong, W.-L., Yao, H., Lepland, A., Klug, M., Eichinger, F., et al. (2021). Methane Transport and Sources in an Arctic Deep-Water Cold Seep Offshore NW Svalbard (Vestnesa Ridge, 79°N). *Deep-Sea. Res. I.: Oceanogr. Res. Pap.* 167, 103430. doi: 10.1016/j.dsr.2020.103430

Schuur, E. A. G., McGuire, A. D., Schädel, C., Grosse, G., Harden, J. W., Hayes, D. J., et al. (2015). Climate Change and the Permafrost Carbon Feedback. *Nature* 520, 171–179. doi: 10.1038/nature14338

Shakhova, N., Semiletov, I. and Panteleev, G. (2005). The Distribution of Methane on the East Siberian Arctic Shelves: Implications for the Marine Methane Cycle. *Geophys. Res. Lett.* 32, L09601. doi: 10.1029/.2005GL02275

Shakhova, N., Semiletov, I., Salyuk, A., Yusupov, V., Kosmach, D. and Gustafsson, O. (2010). Extensive Methane Venting to the Atmosphere From Sediments of the East Siberian Arctic Shelf. *Science* 327, 1246–1250. doi: 10.1126/science.1182221

Sibuet, M. and Olu, K. (1998). Biogeography, Biodiversity and Fluid Dependence of Deep-Sea Cold-Seep Communities at Active and Passive Margins. *Deep-Sea. Res. II.: Top. Stud. Oceanogr.* 45, 517–567. doi: 10.1016/S0967-0645(97)00074-X

Stadnitskaia, A., Ivanov, M. K. and Sinninghe Damsté, J. S. (2008). Application of Lipid Biomarkers to Detect Sources of Organic Matter in Mud Volcano Deposits and Post-Eruptional Methanotrophic Processes in the Gulf of Cadiz, NE Atlantic. *Mar. Geol.* 255, 1–14. doi: 10.1016/j.margeo.2007.11.006

Suess, E. (2014). Marine Cold Seeps and Their Manifestations: Geological Control, Biogeochemical Criteria and Environmental Conditions. *Int. J. Earth Sci.* 103, 1889–1916. doi: 10.1007/s00531-014-1010-0

Sultan, N., Bohrmann, G., Ruffine, L., Pape, T., Riboulot, V., Colliat, J. L., et al. (2014). Pockmark Formation and Evolution in Deep Water Nigeria: Rapid Hydrate Growth Versus Slow Hydrate Dissolution. *J. Geophys. Res. Solid. Earth.* 119, 2679–2694. doi: 10.1002/2013JB010546

Torres, M. E., Collett, T. S., Rose, K. K., Sample, J. C., Agena, W. F. and Rosenbaum, E. J. (2011). Pore Fluid Geochemistry From the Mount Elbert Gas Hydrate Stratigraphic Test Well, Alaska North Slope. *Mar. Petrol. Geol.* 28, 311–331. doi: 10.1016/j.marpetgeo.2009.10.001

Torres, M. E., Tréhu, A. M., Cespedes, N., Kastner, M., Wortmann, U. G., Kim, J. H., et al. (2008). Methane Hydrate Formation in Turbidite Sediments of Northern Cascadia, IODP Expedition 311. *Earth Planet. Sci. Lett.* 27, 170–180. doi: 10.1016/j.epsl.2008.03.061

Ussler, W.III. and Paull, C. K. (1995). Effects of Ion-Exclusion and Isotopic Fractionation on Pore-Water Geochemistry During Gas Hydrate Formation and Decomposition. *Geo-Mar. Lett.* 15, 37–44. doi: 10.1007/BF01204496

Ussler, W.III. and Paull, C. K. (2001). "Ion Exclusion Associated With Marine Gas Hydrate Deposits," in *Natural Gas Hydrates: Occurrence, Distribution, and Detection*. Eds. Paull, C. K. and Dillon, W. P. (Washington, D.C: American Geophysical Union), 41–51.

Waage, M., Portnov, A., Serov, P., Bünz, S., Waghorn, K. A., Vadakkepuliyambatta, S., et al. (2019). Geological Controls on Fluid Flow and Gas Hydrate Pingos Development on the Barents Sea Margin. *Geochem. Geophys. Geosyst.* 20, 630–650. doi: 10.1029/2018GC007930

Werne, J. P., Baas, M. and Sinninghe Damsté, J. S. (2002). Molecular Isotopic Tracing of Carbon Flow and Trophic Relationships in a Methane-Supported Benthic Microbial Community. *Limnol. Oceanogr.* 47, 1694–1701. doi: 10.4319/lo.2002.47.6.1694

Westbrook, G. K., Thatcher, K. E., Rohling, E. J., Piotrowski, A. M., Pälike, H., Osborne, A. H., et al. (2009). Escape of Methane Gas From the Seabed Along the West Spitsbergen Continental Margin. *Geophys. Res. Lett.* 36, L15608. doi: 10.1029/2009GL039191

Conflict of Interest: The authors declare that the research was conducted in the absence of any commercial or financial relationships that could be construed as a potential conflict of interest.

Publisher's Note: All claims expressed in this article are solely those of the authors and do not necessarily represent those of their affiliated organizations, or those of the publisher, the editors and the reviewers. Any product that may be evaluated in this article, or claim that may be made by its manufacturer, is not guaranteed or endorsed by the publisher.